ACS APPLIED MATERIALS & INTERFACES

Research Article

www.acsami.org

Electron-Donor and -Acceptor Agents Responsible for Surface Modification Optimizing Electrochemical Performance

Wail Al Zoubi, Muhammad Prisla Kamil, Hae Woong Yang, and Young Gun Ko*

Materials Electrochemistry Group, School of Materials Science and Engineering, Yeungnam University, Gyeongsan 38541, Republic of Korea

ABSTRACT: The electrochemical roles of electron-donor and -acceptor agents in surface reforming of magnesium alloy were investigated via plasma electrolysis. The surface modification was performed in an aluminate-based electrolyte, having urea and hydrazine with inherent molecular structures, which might act as electron acceptor and donor during plasma-assisted electrochemical reaction. The presence of hydrazine working as donor would promote the formation of magnesium aluminates in the oxide layer, resulting in superior compactness of the oxide layer to that when urea was used as the working as acceptor since the precipitation of $MgCO_3$ was favored in the electrolyte with urea. The thickness of the oxide layer formed by a combination of urea and hydrazine was higher than urea, while the porosity was higher than hydrazine. The electrochemical performance was enhanced in the order of hydrazine, urea and hydrazine combined, and urea, which was discussed on the basis of impedance interpretation.

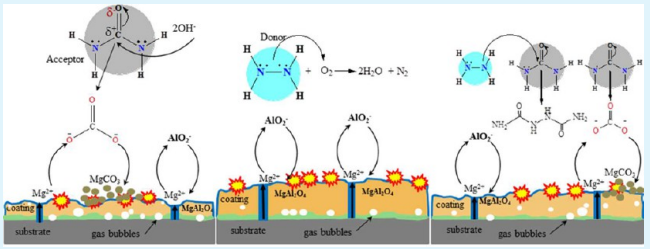

KEYWORDS: *magnesium alloy, oxide layer, acceptor, donor, electrochemistry*

1. INTRODUCTION

Plasma electrolytic oxidation (PEO) has been the subject of recent study for electrochemical coating applications. In general, PEO has long been regarded as one of the eco-friendly wet-coating methods desirable for modifying the surface structure and compounds in various metallic materials to improve electrochemical surface properties by generating denser and more adhesive oxide layer as compared to conventional anodizing methods.[1,2] Previous studies on the PEO-treated materials have reported the formation and structure of the oxide layers produced through the plasma-enhanced electrochemical reactions.[3−10] The characteristics of the oxide layers would depend primarily on electrolyte conditions, such as chemical compositions and their concentrations, as well as electrical variables, such as current density, frequency, etc. Among them, a role of the chemical composition of the electrolyte on the formation of the oxide layer for magnesium alloys has reported to be of great significance. At present, a hierarchy of the inorganic electrolytes, such as aluminate,[11,12] silicate,[13] borate, and phosphate,[14] with different chemical additives were reported to be beneficial for producing the oxide layers on magnesium alloys. In this work, we introduced electron donors as powerful electron-reducing agents in electrochemical reactions and a dense and stable dielectric layer and explored the novel phenomena that could be observed in the plasma-enhanced electrochemical system.

Hydrazine and urea have exhibited good solubility in water and polar solvents, such as C_2H_5OH, DMSO (dimethyl sulfoxide), and DMF (dimethylformamide) because of their high dielectric constant and polarity. Thus, in the literature, the majority of studies regarding the electrochemical roles of donor and acceptor agents on PEO coating reaction have focused on electrical or optical responses, while only a few reports have been made to explore electrochemical behavior. For instance, Bai et al. revealed, on the basis of plasma electrolysis of magnesium alloy in the silicate-phosphate electrolyte with $(CH_2)_6N_4$ working as electron donor, that the formation of the microdefects in the oxide film was inhibited sufficiently to enhance the anticorrosion properties through surface modification mechanism which would allow donor of $(CH_2)_6N_4$ to provide a number of electrons to the electrolyte, transforming O_2 gases into particular water molecules during electrochemical process.[15] In addition, some recent studies have reported that nitrogen might contribute to the growth behavior of the oxide layer by adding donor−acceptor agents, such as H_2NCONH_2, $NaNO_2$, $NaNO_3$, or NH_4NO_3, to the aqueous electrolytes.[16−18] Shang et al. suggested that the addition of sodium nitrite to the sodium-aluminate electrolyte would result in the increase of the layer thickness as well as the decrease of the porosity.[19] The effect of $NaNO_2$ was attributed to oxidation enhancement, not to nitridation.[19]

On the other hand, carbonyl compound with the chemical formula of $CO(NH_2)_2$ often possessed resonance structures that affected its reactivity because oxygen was more electronegative than carbon in nature. This relative electronegativity

Received: April 25, 2017
Accepted: August 3, 2017
Published: August 3, 2017

DOI: 10.1021/acsami.7b05773
ACS Appl. Mater. Interfaces 2017, 9, 28967−28979

would draw electron density away from carbon, causing the increment of the bond's polarity, which thereby made carbon an electrophile working as electron acceptor. On the other hand, amine groups contained a basic nitrogen atom with a line pair (i.e., N_2H_4); thus, during the electrochemistry reactions, the carbon−oxygen double bond might be broken, and the carbonyl group would undergo additional chemical reactions. These reactions were established as addition−elimination or condensation that raised the unresolved question on whether the presence of carbonyl (electron acceptor−donor) or amine (electron donor) groups would be an opportunity or a constraint for coating growth behavior by PEO? Prior to the present investigation, the structure−property information regarding how the additions of carbonyl compound (urea), noncarbonyl compound (hydrazine), or a mixture of two compounds to an alkaline aluminate electrolyte will affect the microstructure and electrochemical response of the oxide layers on magnesium alloys subjected to PEO coatings has been documented rarely. In the present work, the influences of urea, hydrazine, and a mixture of the two compounds on PEO-coating process, coating morphology, phase composition, and corrosion behavior of magnesium alloy is discussed.

2. MATERIALS AND METHODS

2.1. Sample Preparation and PEO Coating. A plate-type sample of the AZ31 Mg alloy with a chemical composition of 3.08 wt % Al, 0.76 wt % Zn, 0.15 wt % Mn, and balanced Mg were used as substrates in this research. Before PEO coating, the surface of the sample was ground and polished in distilled water with SiC emery papers of 400, 800, 1000, 1200, and finally 2400 grit, rinsed with deionized water and cleaned ultrasonically with ethanol. For PEO coating, the composition and concentration of four different electrolytes used in this study were prepared as tabulated in Table 1. Briefly, the compositions of the present electrolytes were KOH + $NaAlO_2$ + glycerin together with urea, hydrazine, and a mixture of urea and hydrazine, which were designated as baths B, C, and D, respectively. Bath A without chemical additive was used to study the influences of urea and hydrazine working as electron acceptor and donor during the growth of coating. PEO coating was carried out using a 20 kW AC power supply equipped with stirring and cooling systems which would keep a temperature of 288 K to stabilize the electrochemical reactions accompanying plasma discharges. A constant current density of 100 $mAcm^{-2}$ was applied to the sample for 15 min with a frequency of 60 Hz.

Table 1. Composition and Concentration of the Alkaline Aluminate Electrolytes Used for the Present PEO Coatings[a]

electrolyte	KOH	$NaAlO_2$	glycerin	$CH_4N_2O_4$ (urea)	N_2H_4 (hydrazine)
bath A	4	8	4	0	0
bath B	4	8	4	4	0
bath C	4	8	4	0	4
bath D	4	8	4	4	4

[a]Units used in the table are grams per liter ($g\ L^{-1}$).

2.2. Microstructural Characterization. Microstructural observations were carried out using scanning electron microscope (SEM, HITACHI, S-4800) equipped with energy-dispersive X-ray spectroscopy (EDS, HRIBA EMAX). The average thickness of the oxide layer was measured from 10 different areas in the cross-sectional morphologies of the oxide layer. The 3-D topography of the oxide layer was observed through scanning probe microscope (SPM, Being Nano-Instruments LTD, CSPM 5500), and then, the values of root-mean-square (rms) for surface roughness were obtained. The image analyzer was used to measure the average size of the micropores present in the oxide layer. The constituent compounds were analyzed by X-ray diffraction (XRD, RIGAKU, D-MAX 2500) with a step size of 0.05° and a scan range of 20−90°. For compositional analysis, Fourier transform infrared spectroscopy (FT-IR, PerkinElmer Spectrum 100) was used in the wide range of 400 to 4000 cm^{-1} to determine the functional groups of the oxide layer. The chemical composition of the oxide layer was characterized in details via X-ray photoelectron spectroscopy (XPS, VG Microtech, ESCA 2000).

2.3. Electrochemical Evaluation. The electrochemical properties were evaluated in a 3.5 wt % NaCl solution at a pH of 7 utilizing three different electrodes: a coated sample with an exposed area of 1 cm^2 as the working electrode, a platinum plate as the counter electrode, and an Ag/AgCl solution as the reference electrode. The corrosion properties of the oxide layer were evaluated by potentiodynamic polarization and electrochemical impedance tests (Potentiostat, Gamry Instruments, Interface 1000). The polarization curves were measured from −0.3 to 0.3 V with respect to the open circuit potential (OCP) at a scan rate of 1 mVs^{-1}. Electrochemical impedance tests were conducted from 10^6 to 0.1 Hz at an interval of 10 points/decade with a 10 mV rms. Such present electrochemistry tests were repeated 3 times at least to gain the reliability of the experimental results.

3. RESULTS

3.1. Transient Voltage−Time Response. Figure 1 shows the curves of rms voltage as a function of coating time during PEO process in four different electrolytes. Regardless of the electrolyte conditions, these curves could be divided into four different regions based on the development of the oxide layer and appearance of plasma spark. During the first region, the surface of magnesium alloy substrate was instantaneously oxidized to form a thin barrier layer accompanying oxygen evolution reactions. In this region, the voltage increased with increasing time at a constant rate, and plasma discharges were absent on the surface of the substrate. When the voltage reached a critical value, however, a number of the micro-discharges would start to form on the oxide surface where they

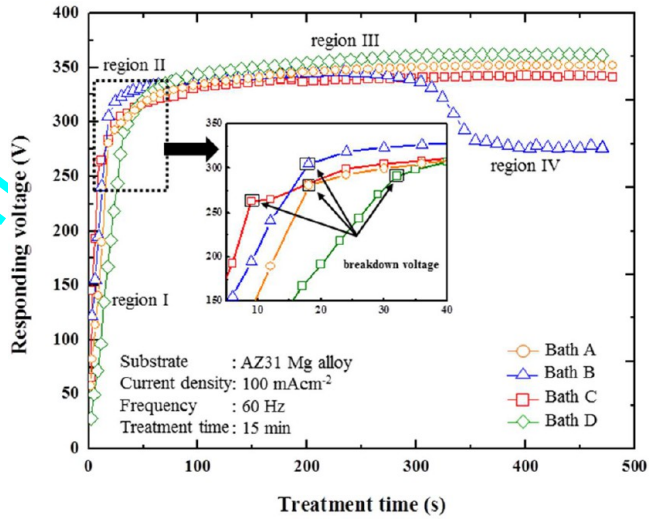

Figure 1. Responding voltage (rms) vs time curves of the AZ31 Mg alloy samples during PEO coatings at 100 $mAcm^{-2}$ in baths A (circle), B (triangle), C (square), and D (rhombus). In region I, the voltage increased linearly because of the occurrence of the passivation film until the breakdown voltage was reached. Sparks begun to appear, so that the oxide layer formed in region II. Appreciable size of discharge spots was noticed in region III. In case of Bath B in region IV, some precipitation of magnesium carbonates would be expected during PEO, resulting in a significant drop in responding voltage.

DOI: 10.1021/acsami.7b05773
ACS Appl. Mater. Interfaces 2017, 9, 28967−28979

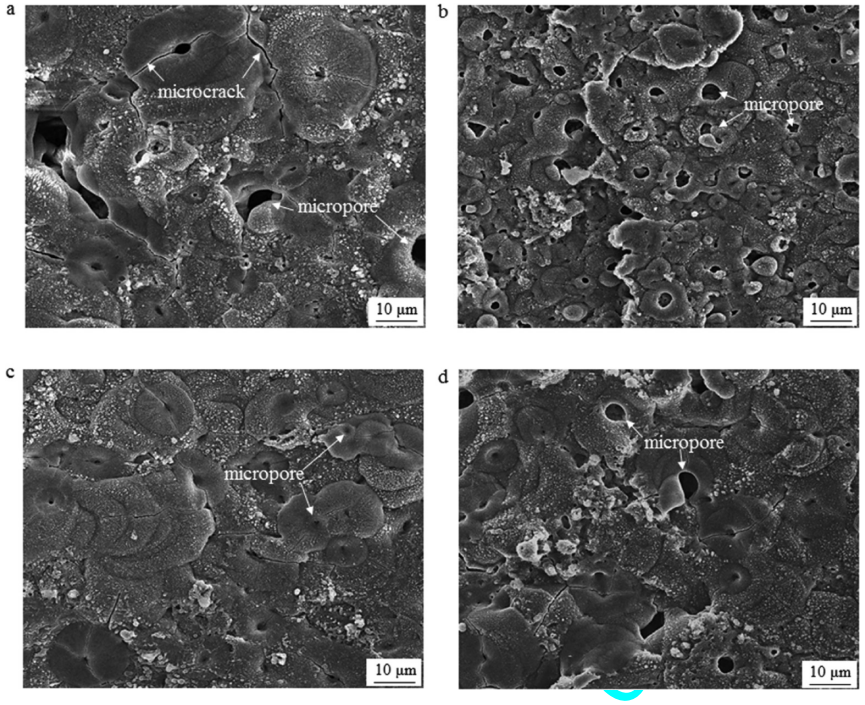

Figure 2. SEM images showing the surface morphologies of the AZ31 Mg alloy samples coated by PEO at 100 $mAcm^{-2}$ for 15 min utilizing four distinctive electrolytes of (a) bath A, (b) B, (c) C, and (d) D. All of the oxide layers presented the porous morphological features with containing the micropores which might be affected by the gas released through the molten oxide and the roles of acceptor and donor agents relating to discharging activity.

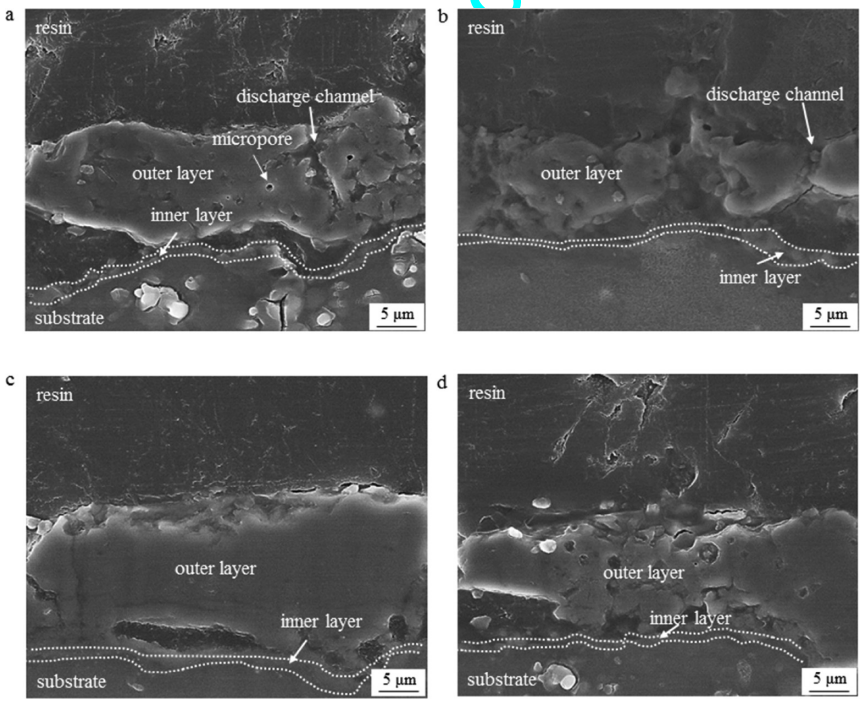

Figure 3. SEM images showing the cross-sectional morphologies of the AZ31 Mg alloy samples coated by PEO at 100 $mAcm^{-2}$ for 15 min utilizing four distinctive electrolytes of (a) bath A, (b) B, (c) C, and (d) D. All of the oxide layers comprised two layers such as outer and inner layers. Some discharge channels, which provided short circuit paths for corrosive ions to infiltrate into the metal substrate, were detected.

showed a tendency to grow in size as the responding voltage increased steadily during PEO. The critical voltage was defined as the breakdown voltage at which the dielectric oxide film was subjected to an electrical breakdown due to impact ionization. PEO process would then enter region II where the increasing rate of voltage decreased appreciably. The development of the individual microdischarges was reported to resort primarily to the electrolyte composition and substrate.[20,21] As shown in Figure 1, the values of breakdown voltage of the samples during PEO process with a couple of chemical additives were in order of hydrazine, mixture of urea-hydrazine, and urea, which were estimated to be ~265, ~290, and ~310 V, respectively. Such

DOI: 10.1021/acsami.7b05773
ACS Appl. Mater. Interfaces 2017, 9, 28967−28979

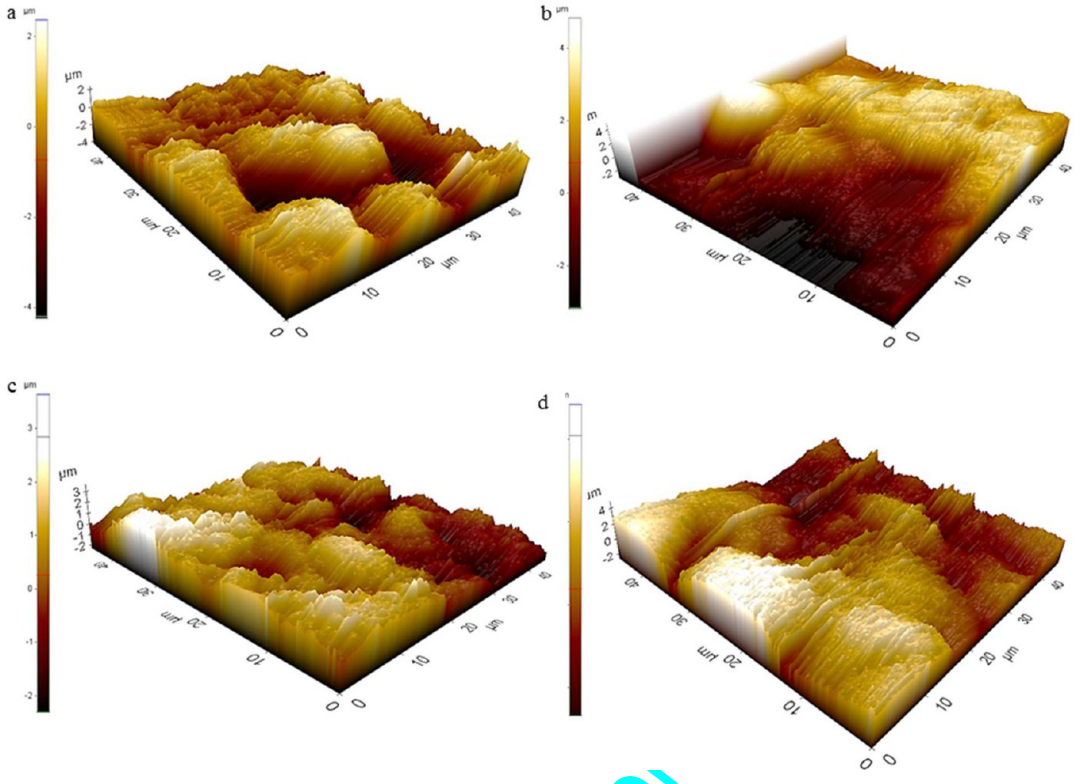

Figure 4. SPM images showing the surface roughness of the AZ31 Mg alloy samples coated by PEO at 100 mAcm^{-2} for 15 min utilizing four distinctive electrolytes of (a) bath A, (b) B, (c) C, and (d) D.

differences in the breakdown voltages were attributed mainly to the variations in the electrolyte composition associated with the additions of urea, hydrazine, and mixture of urea−hydrazine. The breakdown voltage of the sample during PEO coating in the electrolyte with urea was clearly higher than those in cases of hydrazine or the mixture. In addition, the responding voltages of magnesium alloys treated with urea and mixture were higher than that treated with hydrazine. These phenomena suggested that the characteristics of transient voltage during PEO might depend on the chemical stability of the compounds in the alkaline-aluminate electrolyte. In region III, the lifetime and size of the microsparks increased gradually on the entire sample surface which was accompanied by a lower slope of the voltage−time curves as compared to that in region II. In region IV, the appearance of the population of the microsparks decreased significantly while their size and lifetime increased, and their surface color apparently changed from white to orange-red.[22−24]

3.2. Micro-Morphologies of Oxide Layers. Figures 2 and 3 display the SEM images of the surface morphologies and the cross sections of the AZ31 Mg alloy samples treated in baths A−D. The microstructural results show that, regardless of the addition of the chemical additives to the base electrolyte, the oxide layers were observed to exhibit a porous surface morphology. This was due to the active evolution of O_2 and H_2 gases through the decomposition of nitrogen-inducing agents.[25] The oxide layer formed in bath C displayed pretty lower porosity (∼0.78%) than those in bath A (∼2.15%), B (∼2.42%), and D (∼2.25%), indicating that hydrazine would modify the surface topography of the oxide layer. It might be associated with the absence of a cluster of white precipitates in the electrolyte solution. The white precipitates appeared only when urea or/and mixture was added to the electrolyte.[21,26] In addition, the average diameters of the micropores in the oxide layer formed in baths A−D were estimated to be ∼5.6, ∼2.9, ∼2.1, and ∼4.3 μm, respectively. Thus, the additions of donor and acceptor agents to the electrolyte clearly contributed to a significant change in the surface morphologies of the oxide layers. The surface of the oxide layer formed in the electrolyte with hydrazine was homogeneous and compact in nature. Utilizing the electrolyte containing hydrazine, the oxide layer possessed smaller size of the micropores than those formed in baths A, B, and D.[8]

On the other hand, the cross-sectional micrographs in Figures 3a-d revealed that the oxide layer was composed of two layers, such as outer porous layer and inner barrier layer. The thickness of the oxide layers varied with the different electrolyte in the order of baths C > A > D > B due to the different final voltage as shown in the voltage−time curves (Figure 1) as well as the additions of urea, hydrazine, and their mixture to the alkaline-aluminate electrolyte solutions in this study. It might be inferred that PEO in the electrolyte containing urea and magnesium ions would cause the occurrence of the Mg-containing precipitates, which consumed those ions and, thereby, reduced the growth rate of the oxide layer. Figure 3 reveals how the addition of urea affected the thickness of the oxide layer, which would be useful guidance to predict the electrochemical properties.

To examine the surface roughness of the PEO-coated AZ31 Mg alloy samples, evaluations utilizing SPM were made. The results shown in Figure 4 suggested that the surface roughness increased with increasing size and density of the micropores generated inevitably during PEO.

3.3. Chemical Analyses of Oxide Layers. EDS results showing the relative amounts of the elements detected in the AZ31 Mg alloy sample treated in the different electrolytes are

DOI: 10.1021/acsami.7b05773
ACS Appl. Mater. Interfaces 2017, 9, 28967−28979

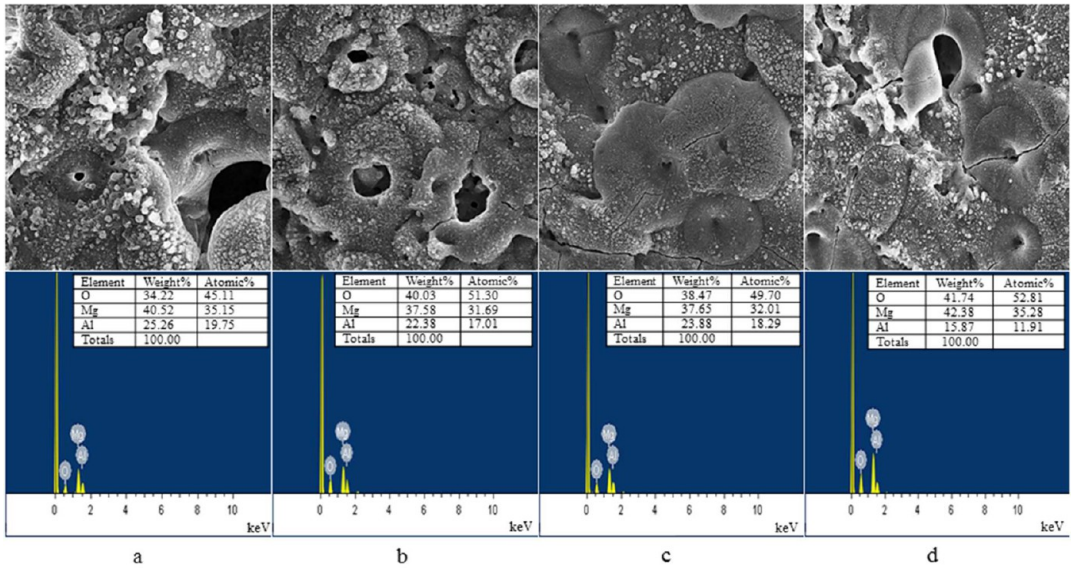

Figure 5. EDS compositional results taken from the oxide layer in the present samples treated in (a) baths A, (b) B, (c) C, and (d) D.

shown in Figure 5. Minor differences were identified in the elemental analyses of the resultant oxide layer. The XRD patterns in Figure 6 showed that $MgAl_2O_4$ (spinel), MgO, and

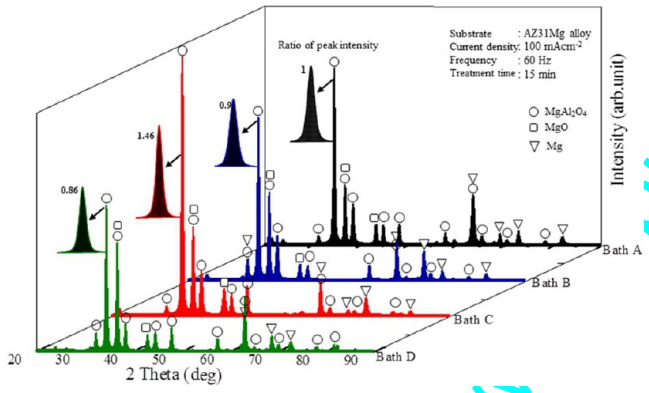

Figure 6. XRD spectra of the present samples treated in (a) baths A, (b) B, (c) C, and (d) D. Cu Kα radiation was used as source. All of the oxide layers constituted $MgAl_2O_4$ and MgO with different ratios of relative peak intensity. The individual peaks of Mg were from the metal substrate.

$Mg(OH)_2$ were the main oxides present in the PEO oxide layers. Based on apparent peak intensities, it was thought that the relative amount of spinel $MgAl_2O_4$ in the oxide layer was the highest when the electrolyte containing hydrazine was employed for PEO. The reason for this behavior was that no white precipitate formed through reactions between hydrazine and AlO_2^-. In the case of bath C, the peaks corresponding to $MgAl_2O_4$ became more intense, which might indicate that X-rays were unable to reach magnesium substrate due to the formation of thicker and more compact coatings as seen from Figure 6. Regarding the relative abundance of the constitutive compounds, the amounts of $MgAl_2O_4$ with and without donor and acceptor in PEO coatings were estimated using the relative peak intensity ratios. The intensity ratios of $(I_{(hydrazine)}/I_{(base)})$ reached ~1.46, which was the highest ratio among the samples in the present study. Khaselev et al. also found that the spinel $MgAl_2O_4$ increased at the expense of MgO during PEO coating of magnesium alloy in an AlO_2^- solution.[27] Further analysis based on FT-IR spectra, as shown in Figure 7a, showed the characteristic absorption bands of HO-Mg−OH and $Al_2O_4^{-2}$. The IR spectrum of the oxide layer exhibited a band at 3400 cm^{-1}, which was assigned to the stretching frequency of the OH group due to the presence of $Mg(OH)_2$ in the oxide layer. In addition, the characteristics of the bands related to M-O stretching modes were noted at 700 cm^{-1}. The representative XPS bands of Al 2p, Mg 1s, and O 1s of the present samples treated in bath D are shown in Figure 7b−d. Mg (1s) core level exhibited a binding energy of 1304 eV (between 1303.5 and 1304.5 eV), demonstrating that the magnesium state existed exclusively in the form of Mg^{2+}, whereas Al (1p) peak for Al compounds was located at 75 eV. As shown in Figure 7b, the oxygen peak in the oxide layer was divided into (O 1s) (530 eV) and (O 1s) (533 eV). These were consistent with the formations of MgO and $MgAl_2O_4$.

3.4. Electrochemical Characterization by Potentiodynamic Polarization. The protective capabilities of the oxide layer were evaluated by potentiodynamic polarization test in 3.5 wt % NaCl solution, and the curves obtained are shown in Figure 8a. The corrosion potential (E_{corr}), and corrosion current density (i_{corr}) drawn from the polarization plots are summarized in Table 2. In a typical polarization curve, positive corrosion potential and/or lower corrosion current density indicated good corrosion resistance with lower corrosion rate. As shown in Figure 9a and Table 2, the oxide layer with hydrazine exhibited higher corrosion potential than those with urea, combination. Furthermore, the corrosion current density (i_{corr}) of the sample with hydrazine was lower by several orders of magnitude as compared to the bare substrate. To quantify the electrochemical differences relatively, the relative efficiency (η) (Table 2) defined as (eq 1)[28] was used.

$$\eta\% = \frac{i_{corr}^0 - i_{corr}}{i_{corr}^0} \times 100 \quad (1)$$

where i_{corr}^0 and i_{corr} are corrosion current densities in solutions without and with donor or acceptor. These results revealed that the corrosion current density decreases remarkably with

DOI: 10.1021/acsami.7b05773
ACS Appl. Mater. Interfaces 2017, 9, 28967−28979

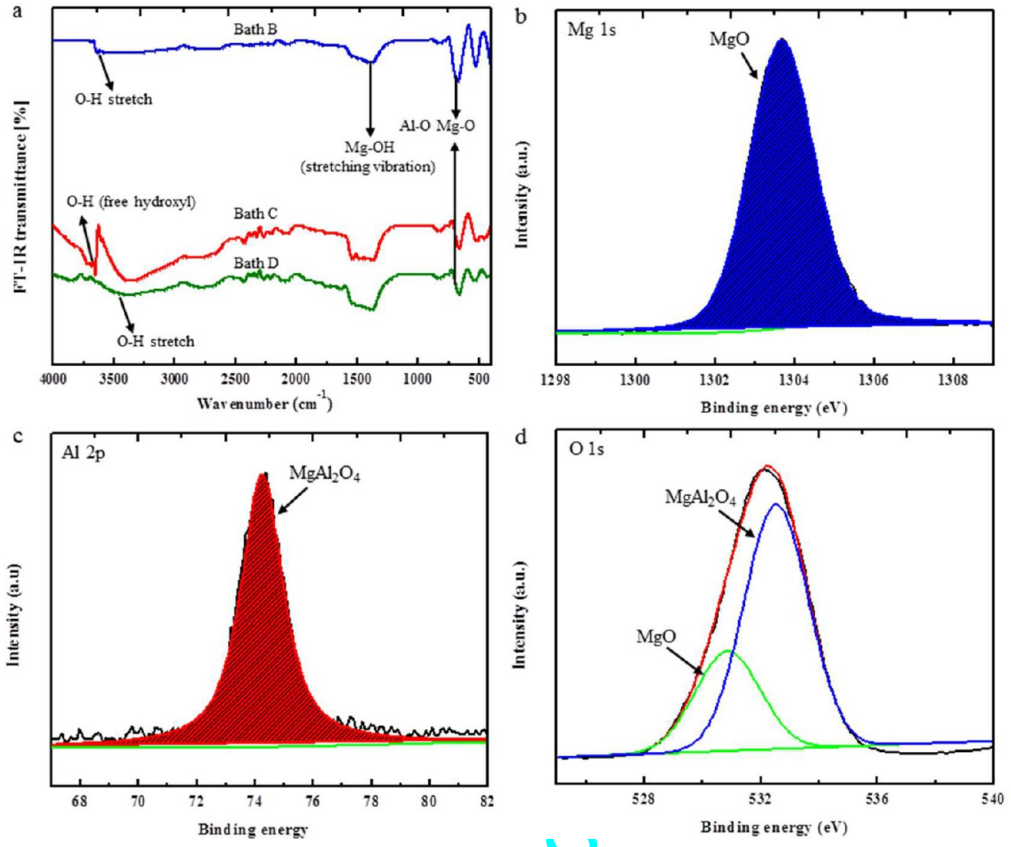

Figure 7. (a) FT-IR spectra of the oxide layers in the present samples treated in baths B, C, and D. The individual bands confirmed the presence of chemical bonding arising from $MgAl_2O_4$ and MgO. XPS spectra of the oxide layers in the present samples treated in bath D as a representative result: (b) Mg 1s, (c) Al 2p, and (d) O 1s. XPS peaks remained constant for all samples.

hydrazine, which led to a clear increase of the relative efficiency to inhibit corrosion process.

On the other hand, the corrosion current density of the PEO-treated magnesium alloys tended to decrease with decreasing surface roughness. The sample with a mean surface roughness (R_a) of ~1.82 μm had the corrosion current density of 21.7 μAcm^{-2} while the sample with R_a of ~0.79 μm exhibited a remarkably low corrosion current density of 26×10^{-3} μAcm^{-2}. This fact suggested that the rough oxide layers might be corresponded to high corrosion current density as observed by several reports.[29,30]

3.5. Electrochemical Characterization by Electrochemical Impedance. The EIS technique was employed to investigate the degradation behavior of the Magnesium alloy in a physiological environment. When the magnesium alloy was exposed in NaCl solution for 4 h, the curves of the Nyquist plot began to become smaller. The EIS spectra of AZ31 Mg alloy are normally characterized by three well-defined loops, but the plot only displayed one high-frequency capacitance loop, and one low-frequency inductance loop, suggesting two different-time constants. However, the medium frequency capacitive loop disappeared in the present study. The high frequency capacitance loop and the low frequency capacitive loop represented the properties of the electric double layer formed at the interface between the metal surface and corrosive medium,[31−35] and the product layer on electrode, respectively.[38] The hydrazine coating provides the highest corrosion resistance of all the samples, which can be identified by the largest capacitive loop and the highest impedance magnitude ($|Z|_{f\to 0}$) in Figure 8b–d.

To analyze the EIS spectra of the AZ31 Mg alloy, an equivalent circuit model shown in Figure 8b, was proposed. The model was based on the impedance plots and the EIS studies of Gao et al., Baril et al., Liang et al., and Song et al. on the PEO coating to explain the corrosion behavior of Mg alloy.[37,39−41] In the circuit R_s represents the corrosion resistance of the NaCl solution between the sample and counter electrode, and the outer porous coating and the passive film were represented respectively by the first resistance (R_1) and the constant phase element (CPE1). In addition, R_2 represents the contribution of the inner barrier region to the overall corrosion resistance (Figure 8b) and the corresponding capacitance is represented by CPE2. R_3 and L are in series to represent the inductive impedance behavior, where R_3 represents the resistance of the corrosion products and L describes the corrosion behavior at low frequencies.[36] Table 3 shows the EIS fitting data obtained from the fitting of the equivalent circuits and the experimental values obtained from the impedance data.

3.6. Effects of Donor and Acceptor Concentrations. Figure 9 presents the variations of the thickness values of the oxide layers formed via PEO with respect to the concentrations of acceptor (urea) and donor (hydrazine) agents in the alkaline-aluminate electrolyte. It was apparent that the thickness of the oxide layer decreased with increasing concentration of acceptor which absorbed Mg^{2+} ions traveling within the electrolyte through the cation−anion pair chemical reactions. This coincided with a sudden increase in the amount of magnesium carbonate when the concentration of acceptor increased from 2 to 8 g L^{-1}. Thus, magnesium carbonate was

DOI: 10.1021/acsami.7b05773
ACS Appl. Mater. Interfaces 2017, 9, 28967−28979

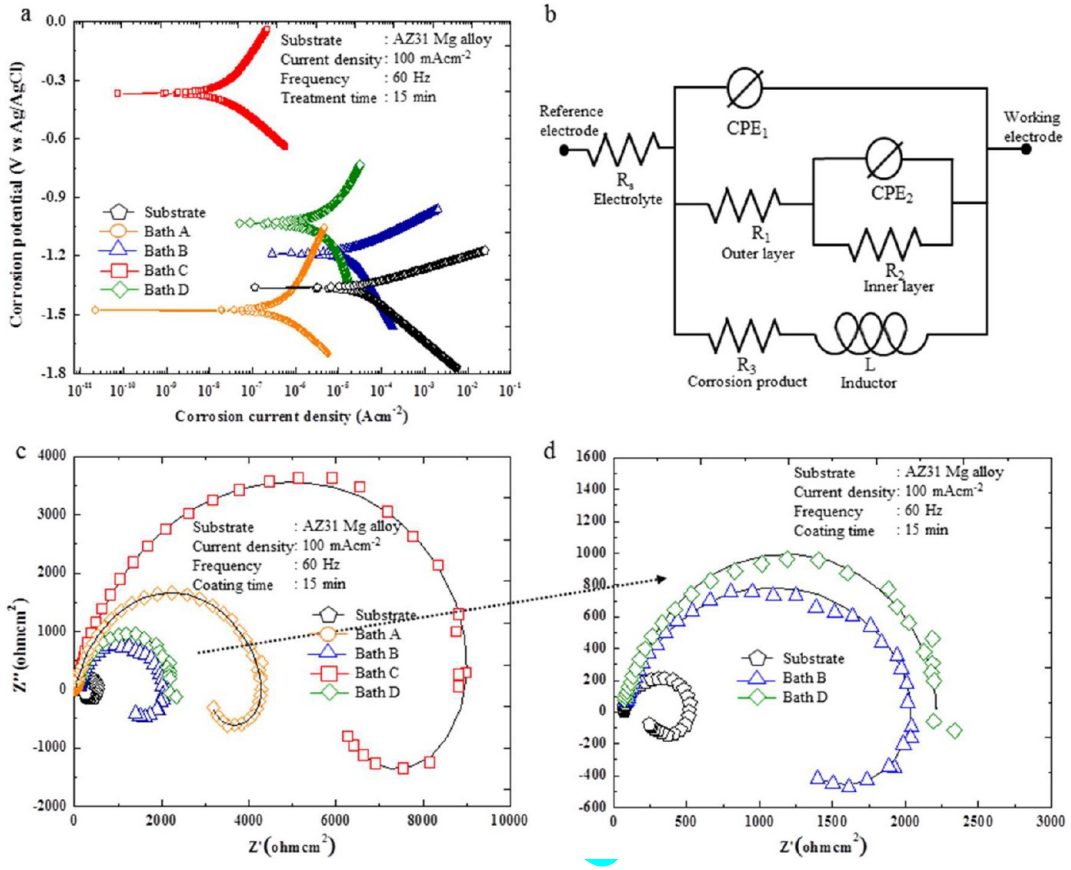

Figure 8. (a) Potentiodynamic polarization curves of the present samples treated in baths A–D. (b) Equivalent circuit model consisting of two capacitive loops to describe the electrochemical characteristics of the inner and outer layers. An inductive loop was associated with corrosion products. (c) Nyquist plots of the present samples treated in baths A–D. (d) High-resolution EIS plots of baths B and D. All electrochemical characterizations confirmed that the sample treated in bath C exhibited superior corrosion resistance owing to the role of hydrazine working as electron donor.

Table 2. Potentiodynamic Polarization Results of the Samples Treated by PEO Coatings Measured from −0.3 to 0.3 V versus the Open Circuit Potential in 3.5 wt.% NaCl Solution

sample	E_{corr} (V)	I_{corr} (μAcm^{-2})	corrosion rate (mpy)	relative efficiency (%)
AZ31 Mg alloy	−1.36	33.4	40	-
bath A	−1.48	0.670	0.30	97
bath B	−1.19	21.7	26	35
bath C	−0.36	26.1 × 10^{-3}	0.03	99
bath D	−1.03	13.6	16	59

generated through chemical reactions between acceptor and Mg^{2+} ions which would be triggered by intense thermal energy of PEO accompanying microdischarge.[42,43] This might account for the formation mechanism of the oxide layer where a significant decrease in the thickness of the oxide layer as the concentration of acceptor changed from 4 to 8 g L^{-1}. In addition, Figure 9 might suggest that PEO energy would be more or less converted to either the decomposition of acceptor agent or the chemical reaction between acceptor and Mg^{2+} ions. Both cases would lead to a decrease in the thickness of the resultant oxide layer. PEO coating treated in the electrolyte containing acceptor agent differed from the case treated with donor agent. Bath C with hydrazine resulted in the different

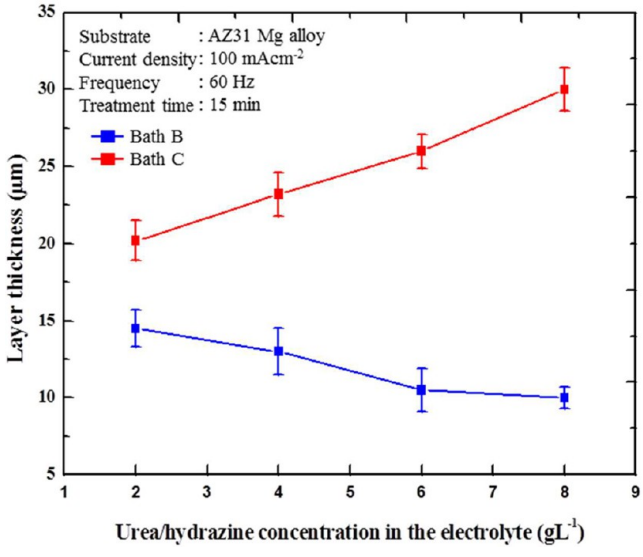

Figure 9. Variation of thickness in the oxide layers with respect to the concentrations (2–8 g L^{-1}) of urea and hydrazine in the present electrolyte.

growth behavior where the thickness of the oxide layer increased with increasing concentration of hydrazine.

Figure 10 presents the potentiodynamic polarization curves of the present samples when the different concentrations of

DOI: 10.1021/acsami.7b05773
ACS Appl. Mater. Interfaces 2017, 9, 28967–28979

Table 3. Electrochemical Impedance Results of the Samples Treated by PEO Coatings in Baths A–D[a]

sample	R_1 (Ω cm^2)	R_2 (Ω cm^2)	R_3 (Ω cm^2)	CPE_1-T	CPE_1-P	CPE_2-T	CPE_2-P	L (H/cm^{-2})
AZ31 Mg alloy	475	0.03	236	3.81×10^{-5}	0.93	2.84×10^{-10}	0.87	120
bath A	4370	1830	8100	1.84×10^{-3}	0.88	1.58×10^{-6}	0.82	3750
bath B	845	1230	2170	1.11×10^{-5}	0.83	3.77×10^{-9}	0.11	2000
bath C	8820	1100	15100	2.86×10^{-6}	0.83	2.19×10^{-5}	0.98	5180
bath D	692	2480	6640	2.30×10^{-6}	0.99	2.28×10^{-6}	0.95	0.09

[a]All values are estimated by the analysis in the context of the equivalent circuit model.

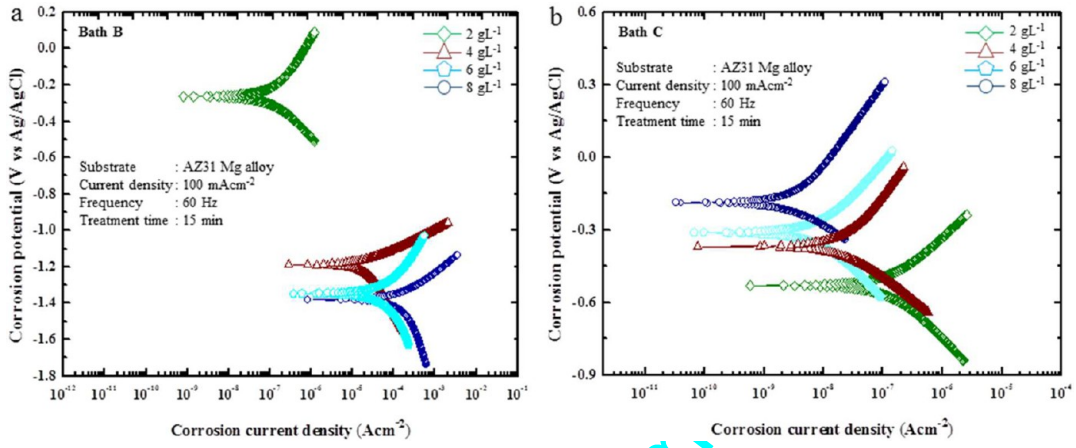

Figure 10. Potentiodynamic polarization curves of the present samples treated in (a) baths B and (b) C with respect to the concentrations of urea and hydrazine in the present electrolyte.

urea and hydrazine were added into the electrolyte. Regardless of the concentration of urea working as electron acceptor, the polarization curves were in parallel with each other, implying that the cathodic and anodic reactions were not affected by the concentration of the acceptor agent. It was obvious from Figure 10a that the higher concentration of acceptor, the higher corrosion current densities in the polarization curves, as seen from in Table 4. Higher concentration of acceptor agent would

Table 4. Potentiodynamic Polarization Results of the Samples Treated by PEO Coatings in Baths B and C with Respect to Concentrations of Urea (Acceptor) and Hydrazine (Donor)

sample	concentration (g L^{-1})	E_{corr} (V)	i_{corr} (μA cm^{-2})
bath B (urea)	2	−264	0.16
	4	−1.19	22
	6	−1.35	67
	8	−1.38	2.1×10^2
bath C (hydrazine)	2	−530	0.14
	4	−0.360	2.6×10^{-4}
	6	−0.311	9.9×10^{-5}
	8	−0.191	3.8×10^{-5}

be likely to cause a decrease in the intensity of ion transfer at the electrolyte/oxide interface, so that the decrease in growth rate of the oxide layer was attained. On the other hand, Figure 10b reflected that the current densities showed a decreasing tendency with higher concentration of donor agent which reached a minimal value at 8 g L^{-1}. This phenomenon was attributed to the increase in the chemical reactivity by the concentration of donor agent.

3.7. Comparison with Other Surface Modification Methods. To compare the present results with the electrochemical properties of the same-classified AZ31 Mg alloys coated by other surface treatment methods, the electrochemical results via hydrothermal treatment,[44] hydrophobic coating,[45] superhydrophobic,[44] hybrid coating,[46,47] sol–gel coating,[48] metallic coating,[49] anodizing coating,[50] and PEO coating[51,52] are illustrated together in Figure 11. Several aspects from such comparison were drawn. First, it was clear from Figure 11 that

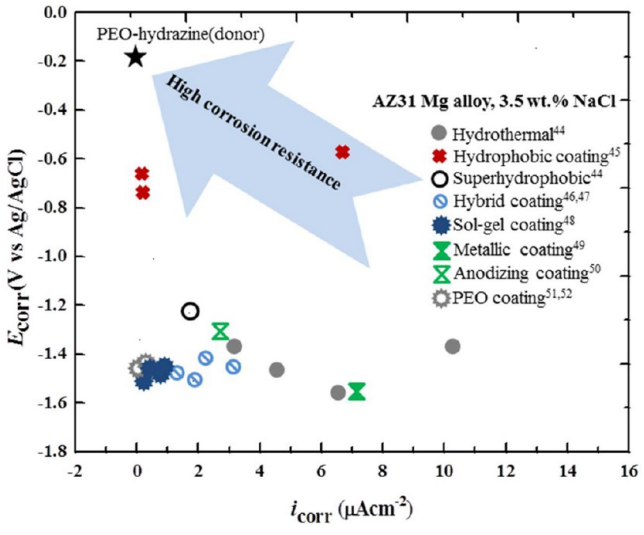

Figure 11. Comparison of E_{corr} and i_{corr} values of the AZ31 Mg alloy samples treated by several surface modification methods, such as hydrothermal,[44] hydrophobic coating,[45] superhydrophobic,[44] hybrid coating,[46,47] sol–gel coating,[48] metallic coating,[49] anodizing coating,[50] and PEO coating.[51,52] The present result was the case in bath C containing hydrazine, which was most desirable in this study. The electrolyte used for all results was 3.5 wt % NaCl solution.

DOI: 10.1021/acsami.7b05773
ACS Appl. Mater. Interfaces 2017, 9, 28967–28979

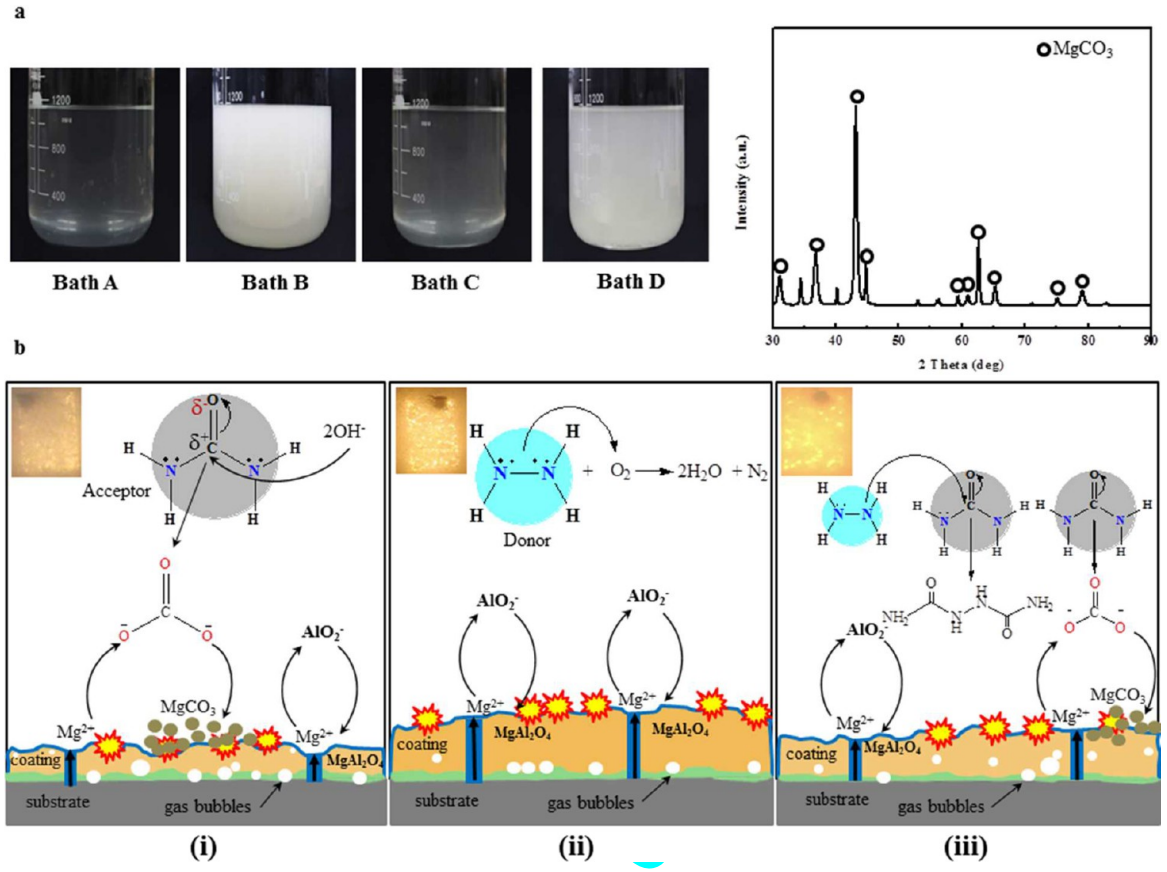

Figure 12. (a) Photographic observations of the eletrolytes after PEO to see whether the precipation of $MgCO_3$ took place or not. XRD data confirmed the formation of $MgCO_3$ only in baths B and D. (b) schematic diagram underlying the core mechanism to describe the development of the oxide layers in (i) bath B with urea (ii), bath C with hydrazine, and (iii) bath D with mixture by taking the roles of electron acceptor and donor during plasma-assisted electrochemical reactions into account.

the oxide layer based on the present strategies utilizing the addition of hydrazine working as electron donor exhibited the lowest value of i_{corr} when compared to the other methods. Second, the value of E_{corr} of the PEO-hydrazine case was more positive than those reported by the others. The comparison of these results led to the conclusion that PEO coating with the presence of hydrazine donor agents would provide excellent protective coating for magnesium-based alloys. This finding would be explained by the sufficient growth of the oxide layer on the metal anode when a number of electrons provided by donor agent would contribute to plasma-assisted electrochemical reactions to the oxide layer during PEO.

4. DISCUSSION

4.1. Chemical Roles of Acceptor and Donor. The reactivity of carbonyl compounds would rely chemically on the group attached directly onto carbon atom working as electron acceptor, which was ascribed to the resonance-stabilized structures to donate a number of electrons by the specific group from oxygen atom. The strong resonance-stabilized structure led to the increase in the stability of carbonyl compounds. As carbonyl compounds possessed the stable bonds in nature and the energies for their formations were known to be pretty high, carbon atom would be attacked with ease by either donor nucleophiles (e.g., negatively charged ions like OH^-) or a negatively charged part of another molecules (e.g., the lone pair electrons of nitrogen atom in the hydrazine molecule). This fact might render the formation of carbonyl groups in organic compounds to be thermodynamically favorable, so that the creation of carbonyl bond as the end product would drive a chemical reaction for the formation of newly fomed compounds for different purposes. This led to an unresolved question on whether the absence of stable carbonyl groups in organic compounds would be beneficial for improving the electrochemical performance of the magnesium alloy subsequent to PEO coating?

4.2. Microstructural Interpretation by Considering Roles of Acceptor and Donor. Adding donor−acceptor agents into the electrolyte clearly influences the initiation and growth of the oxide layers. Under the constant current mode, the voltage increased earlier and faster in the presence of acceptor−donor agents (stable carbonyl group). In the case of the constant current regime, the voltage increased more quickly before the breakdown potential was exceeded and reached higher breakdown voltage values with urea. Such differences in the breakdown voltage were mainly attributed to variations in the electrolyte composition associated with CH_4N_2O (carbonyl compounds), N_2H_4 (donor), or their mixture (acceptor−donor). The breakdown voltage of the sample during PEO coatings in CH_4N_2O was clearly higher than those during PEO coatings in hydrazine and the mixture. These different breakdown voltages revealed that the plasma chemical reactions at the magnesium alloy/electrolyte interface were quite different in the present of carbonyl compounds. In other word, the voltage of the magnesium alloy treated in the CH_4N_2O was lower in the fourth stage. This was attributed to

DOI: 10.1021/acsami.7b05773
ACS Appl. Mater. Interfaces 2017, 9, 28967−28979

the drastic reduction in the electrolytic magnesium, which coincided with the sudden increase of carbonate precipitates ($MgCO_3$) (as shown in Figure 12a) in the solution.[31] Figure 12a shows the X-ray diffraction patterns of the dried powders, collected from precipitates in baths B and D. The precipitate was formed due to the decomposition of the urea by thermal analysis and therefore the amount of this precipitates increases with rise of the temperature and reaction time. During this period, this voltage was directly correlated with a change in the optical and acoustic characteristics of the discharge, a change in the surface properties, and carbonate precipitation (Figure 12a).[23,24] The trends indicated that adding hydrazine produces coatings with higher electrical resistivity and the growth of oxide layer against voltage flow. This improvement was also indicated by in the higher initial impedance values during corrosion testing. With the present of hydrazine, microcracks on surface of this oxide layer also increased, which was due to the high-temperature gradients between the cool electrolytes and the discharge channels. We concluded the different chemical composition such as high electron donor for amino groups led to a significant change in the surface morphologies of the oxide layers.

On the basis of the SEM and EDS analyses assuming the electrolytic magnesium was the only source for layer growth on the surface, the consumed magnesium of electrolyte will be found in the precipitate or layer growth (Figure 2b). Thus, the precipitate affected the layer thickness, which incompletely protected of the surface of those samples after 15 min in baths A−D. Evidently, a portion of the plasma energy could be diverted into urea decomposition or reactions between urea and magnesium or into precipitate activation, leading to weakening microarc intensity.[19,31]

On the basis of the above observation, we proposed two plausible reasons explanations for this difference in the microstructure. First, the hydrazine could require less energy to decompose compared with urea (eqs 18 and 19), the end of at this section. Second, the wider pores and higher porosity in the samples that used urea, hydrazine, and urea-hydrazine mixture could thus be attributed to the decomposition and reactions of these compounds in solution, which creates fewer long-lived sparks. Our results were thus in good agreement with previous studies.[19,31] On the other hand, reactions 2−5 below indicated that Al_2O_3 was first produced during the high-temperature PEO process, and then reacted with MgO to form $MgAl_2O_4$.[34]

$$NaAlO_2 + 2H_2O \rightarrow Al(OH)_4^- + Na^+ \quad (2)$$

$$4Al(OH)_4^{-1} - e \rightarrow 4Al(OH)_3 + 2H_2O + O_2 \quad (3)$$

$$2Al(OH)_3 \rightarrow 4Al_2O_3 + 3H_2O \quad (4)$$

$$Al_2O_3 + MgO \rightarrow MgAl_2O_4 \quad (5)$$

Combined with the results of EDS and XRD, a good agreement was identified that Al and Mg were present in the oxide layer. Therefore, $Mg(OH)_2$ exhibited the highest peak from bath C, causing NH_3 to be generated through the reaction between urea and water. This reaction formed an equivalent of ammonia and one equivalent of carbamic acid. Moreover, the acid rapidly decomposes to form gaseous carbon dioxide and another equivalent of ammonia, so the pH electrolyte will become higher.[21] However, the EDS results exhibited the element distribution in and around the pores, as shown in Figure 4. This figure shows that the Mg concentration in the pores was obviously much higher than that around the micropores, while the Al content in the particles was richer than that in the micropore.

4.3. Electrochemical Behavior by Considering Roles of Acceptor and Donor. The results indicated based on the present electrochemical assessments that the anticorrosion properties of the AZ31 Mg alloy substrate were improved greatly by the PEO coatings formed in a sodium aluminate electrolyte with hydrazine additive.[33] This was because the increasing fraction of $MgAl_2O_4$ in the oxide layer contributed to the better corrosion resistance of the sample coated in the hydrazine-PEO electrolyte. The presence of spinel $MgAl_2O_4$ was beneficial for improving the corrosion resistance of the oxide coating formed on the AZ31 Mg alloy.[36] Moreover, the sample coated in bath C showed higher resistance against transportation of corrosive Cl^- to the magnesium substrate.

The worst corrosion resistance was observed for the bare AZ31 Mg alloy, exhibiting the smallest semicircle in the complex plot. Thus, the corrosion resistance of the alloy could be significantly improved by all the coatings studied herein. However, the acceptor−donor coating showed better corrosion resistance than the acceptor coating, as indicated by the lower shrinkage in Figure 8c and d.

Generally, higher R_1 values are accompanied by lower corrosion rates of the corroding alloy. In this regard, the N_2H_4-coated sample was expected to have the lowest corrosion rate among the tested samples, as shown by its highest R_1 value (8820 Ω m^2) (Table 3) and lowest corrosion rate (0.03 mpy) (Table 1).[53] The evolution of the empirical constant indicated that the empirical constant of CPE1-P, remains higher than 0.8 throughout sample immersion for up to 4 h, indicating distorted capacitance behavior of the outer porous coating.[54] Therefore, the values of CPE2-P for the sample were almost the same at ∼0.8 (Table 3) indicating a distorted diffusion behavior, which explained the penetration of NaCl solution toward the magnesium alloy through the diffusion process.[55]

4.4. Formation Mechanism for Inorganic Oxide Layer. Previous studies have indicated that the major components in electrolytes based on magnesium and sodium aluminate are $MgAl_2O_4$ and MgO.[56] However, the nonexistence of the nitrogen element in the coating, and the $MgAl_2O_4$/MgO ratios suggested that N_2H_4 promoted the chemical reaction to that forms the $MgAl_2O_4$ phase rather than a simple mechanical trapping of the nitrogen element. We propose the following chemical reaction mechanisms. Mg transforms into magnesium ion by loss of electrons and reacted with other ions present in the discharge channels such as O^{2-}, CO_3^{2-}, OH^-, and AlO_2^-, which resulted from the components of the aluminate electrolyte. In this mechanism, both MgO and $MgAl_2O_4$ were formed by outward migration of Mg^{2+} ions from the anode (metal) into the discharge channels and inward migration of O^{2-} and $Mg(OH)^-$ ions from the electrolytic solution into the discharge channels because of the presence of high electric fields between the anode (substrate) and cathode (electrolyte).[57] The formation of MgO and $MgAl_2O_4$ could proceed according to reactions below.

$$Mg \rightarrow Mg^{2+} + 2e \quad (6)$$

$$Mg^{2+} + 2OH^- \rightarrow MgO + H_2O \quad (7)$$

$$NaAlO_2 + 2H_2O \rightarrow Na[Al(OH)_4] \quad (8)$$

DOI: 10.1021/acsami.7b05773
ACS Appl. Mater. Interfaces 2017, 9, 28967−28979

$$Na[Al(OH)_4] \rightarrow Na^+ + Al(OH)_4^- \quad (9)$$

$$Mg^{2+} + 2Al(OH)_4^- \rightarrow MgAl_2O_4 + 4H_2 \quad (10)$$

Through high-temperature oxidation under electrolytic plasma processing, $MgAl_2O_4$ ($MgAl_2O_4$ could also form via the previous reactions 2−5 and MgO could be formed via the following reactions:

$$2Mg + O_2 \rightarrow 2MgO \quad (11)$$

$$MgO + Al_2O_3 \rightarrow MgAl_2O_4 \quad (12)$$

Growth contribution contributes to nitrogen, and oxygen diffusion was a minor process in layer growth. Therefore, their presence could be a critical factor in the strong bonding between the oxide layer and the metal substrate. These suggestions were thus in good agreement with previous studies, which indicated that the products of electrochemical oxidation of urea were carbonates and nitrogen gas (Figure 12b(i)), the electro-oxidation of urea had a standard electrode potential of (E° = 1.147 V).[57−59]

$$CO(NH_2)_{2aq} + 8OH^- \rightarrow N_2 + CO_3^{2-} + 6H_2O + 6e \quad (13)$$

However, H_2NCONH_2 may decompose into equal amounts of NH_3 and cyanic acid (HNCO) (eq 14) at temperatures above 152 °C under certain conditions or react with H_2O to produce NH_3 and CO_2 (eq 15).[60] The HNCO begins to react with undecomposed urea to produce biuret ($NH_2CONHNH_2$) (eq 16) at ∼160 °C. The biuret can react with HNCO via eq 17, to produce ammelide.[61] Previous reports explained that NH_3 dropped fast and CO_2 only at higher temperatures, possibly due to the formation and deposition of $(NH_4)CO_3$ on the flow duct in front of measurement inlet and its evaporation at higher temperatures. However, the main reason for the drop of NH_3 at higher temperatures was the depletion of urea. Moreover, it was also found that at a temperature higher than 350 °C, small amount of NO_x appears under the air atmosphere.[62]

$$N_2H_4CO \rightarrow NH_3 + HNCO \quad (14)$$

$$N_2H_4CO + H_2O \rightarrow 2NH_3 + CO_2 \quad (15)$$

$$N_2H_4CO + HNCO \rightarrow NH_2CONHCONH_2 \quad (16)$$

$$2HNCO + N_2H_4CO \rightarrow \text{ammelide} + 2H_2O \quad (17)$$

Therefore, by PEO coatings in the electrolyte of hydrazine (Figure 12b(ii)), the anodic reaction can proceed via direct pathway (eq 18), hydrazine decomposes directly to N_2 and H_2O; it also decomposes chemically via the indirect pathway (eq 19), to NH_3, N_2, and H_2. In addition, the N_2H_4 emission was very low in air flow in the temperature range of 798−998 °C. The reactions of hydrazine may proceed via other pathways.[57,58]

$$N_2H_4 + 4OH^- \rightarrow N_2 + 4H_2O + 4e \quad (18)$$

$$2N_2H_4 \rightarrow NH_3 + N_2 + H_2 \quad (19)$$

Therefore, N_2H_4 benefitted the layer growth and reduces the layer porosity, which was of importance in generating the oxide layer with fairly high compactness. Therefore, hydrazine is used as an oxygen scavenger in electrolyte solution (the reaction between hydrazine and oxygen in alkaline solution has shown in the Figure 12b(iii). In addition, the decrease in precipitation was accompanied by an increase in layer growth, suggesting the effects of N_2H_4 originate from loss of the carbonyl group Figure 12. This was because the thermal decomposition of hydrazine hydrate will still generate ammonia, but at a much lower level, and the increase in the hydrazine hydrate concentration and the reaction temperature does not result in obvious increase of ammonia emission.[60]

The PEO coatings in bath C (Figure 12b(iii)) also produced gas bubbles, but the amount of gas was less. This could be the reason for the presence hydrazodicarbonamide (HDCA), which was produced by reacting 1 mol of hydrazine with 2 mol of urea.[63,35]

$$H_2NNH_2{\cdot}H_2O + H_2NCONH_2 \rightarrow H_2NCONHNHCONH_2 + 2NH_3{\cdot}H_2O \quad (20)$$

In addition, derivatives of urea as biuret, cyanuric acid, and melamine may proceed via other reactions, which will enhance the polymerization of hydrazine to form branched polymers like polyuria polyol if the proportion of urea is high enough in the mixture.[64]

5. CONCLUSIONS

In this study, the additions of urea ($CO(NH_2)_2$), hydrazine (N_2H_4), and a mixture of urea-hydrazine, which would play as electron acceptor, donor, and combined role, were controlled in the alkaline aluminate electrolyte to look into the microstructural evolution of the oxide layer and related electrochemical properties of magnesium alloy subjected to PEO, and these results were compared to those by the case without chemical additive. Microstructural observation on the micromorphologies of the oxide layer revealed that the additions of urea, hydrazine, and mixture to the present electrolyte gave rise to the significant changes in porosity and surface roughness in the order of bath B (with urea) > bath D (mixture) > bath A (without additive) > bath C (with hydrazine). When hydrazine working as donor was added in the present electrolyte, the oxidation kinetics would be triggered to greater extent than the use of urea absorbing the electron from the plasma-assisted electrochemical reactions during the growth of the oxide layer. In addition, the precipitation of $MgCO_3$ was only favored in the electrolyte containing urea, which would retard the growth of the conformal oxide layer. Thus, the absence of stable carbonyl groups in organic compounds resulted in the decrease in porosity and surface roughness of coating as well as the increase in thickness and relative amount of $MgAl_2O_4$ in the oxide layer. According to the present electrochemical analyses utilizing potentiodynamic polarization and impedance tests in 3.5 wt % NaCl solution, it was concluded that excellent anticorrosion resistance would be optimized by the oxide layer formed in the electrolyte with N_2H_4 inorganic additive working as electron donor.

AUTHOR INFORMATION

Corresponding Author

*E-mail: younggun@ynu.ac.kr. Tel: +82-53-810-2537. Fax: +82-53-810-4628.

ORCID

Wail Al Zoubi: 0000-0002-9959-1431

Notes

The authors declare no competing financial interest.

DOI: 10.1021/acsami.7b05773
ACS Appl. Mater. Interfaces 2017, 9, 28967−28979

■ ACKNOWLEDGMENTS

Financial support from National Research Foundation, Ministry of Education, Republic of Korea (NRF-2017R1D1A1A09000921), was acknowledged.

■ REFERENCES

(1) Li, X.; Liu, X. Y.; Luan, B. L. Corrosion and Wear Properties of PEO Coatings Formed on AM60B Alloy in $NaAlO_2$ Electrolytes. *Appl. Surf. Sci.* **2011**, *257*, 9135−9141.
(2) Dey, A.; Rani, R. U.; Thota, H. K.; Sharma, A. K.; Bandyopadhyay, P.; Mukhopadhyay, A. K. Microstructural, Corrosion and Nanomechanical Behaviour of Ceramic Coatings Developed on Magnesium AZ31 Alloy by Micro Arc Oxidation. *Ceram. Int.* **2013**, *39*, 3313−3320.
(3) Li, Z.; Yuan, Y.; Sun, P.; Jing, X. Ceramic Coatings of LA141 Alloy Formed by Plasma Electrolytic Oxidation for Corrosion Protection. *ACS Appl. Mater. Interfaces* **2011**, *3*, 3682−3690.
(4) Yao, Z.; Jia, F.; Tian, S.; Li, C.; Jiang, Z.; Bai, X. Microoporous Ni-Diped TiO_2 Film Photocatalyst by Plasma Electrolytic Oxidation. *ACS Appl. Mater. Interfaces* **2010**, *2*, 2617−2622.
(5) Al Zoubi, W.; Kamil, M. P.; Ko, Y. G. Synergistic Influence of Inorganic Oxides (ZrO_2 and SiO_2) with N_2H_4 to Protect Composite Coatings Obtained via Plasma Electrolyte Oxidation Mg Alloy. *Phys. Chem. Chem. Phys.* **2017**, *19*, 2372−2382.
(6) Wu, X.; Su, P.; Jiang, Z.; Meng, S. Influence of current Density on Tribological Characteristics of Ceramic Coatings on ZK60 Mg Alloy by Plasma Electrolytic Oxidation. *ACS Appl. Mater. Interfaces* **2010**, *2*, 808−812.
(7) Raj, V.; Mubarak Ali, M. Formation of Ceramic Alumina Nanocomposite Coatings on Aluminum for Enhanced Corrosion Resistance. *J. Mater. Process. Technol.* **2009**, *209*, 5341−5352.
(8) Bala Srinivasan, P.; Blawert, C.; Dietzel, W. Effect of Plasma Electrolytic Oxidation Treatment on the Corrosion and Stress Corrosion Cracking Behaviour of AM50 Magnesium Alloy. *Mater. Sci. Eng., A* **2008**, *494*, 401−406.
(9) Luo, H.; Cai, Q.; Wei, B.; Yu, B.; Li, D.; He, J.; Liu, Z. Effect of $(NaPO_3)_6$ Concentrations on Corrosion Resistance of Plasma Electrolytic Oxidation Coatings Formed on AZ91D Magnesium Alloy. *J. Alloys Compd.* **2008**, *464*, 537−543.
(10) Liang, J.; Guo, B.; Tian, J.; Liu, H.; Zhou, J.; Liu, W.; Xu, T. Effects of $NaAlO_2$ on Structure and Corrosion Resistance of Microarc Oxidation Coatings Formed on AM60B Magnesium Alloy in Phosphate-KOH Electrolyte. *Surf. Coat. Technol.* **2005**, *199*, 121−126.
(11) Sreekanth, D.; Rameshbabu, N.; Venkateswarlu, K. Effect of Various Additives on Morphology and Corrosion Behavior of Ceramic Coatings Developed on AZ31 Magnesium Alloy by Plasma Electrolytic Oxidation. *Ceram. Int.* **2012**, *38*, 4607−4615.
(12) Alabbasi, A.; Bobby Kannan, M.; Walter, R.; StÖrmer, M.; Blawert, C. Performance of Pulsed Constant Current Silicate-Based PEO Coating on Pure Magnesium in Simulated Body Fluid. *Mater. Lett.* **2013**, *106*, 18−21.
(13) Kamil, M. P.; Kaseem, M.; Ko, Y. G. Soft-Plasma Electrolysis With Complex Ions for Optimizing Electrochemical Performance. *Sci. Rep.* **2017**, *7*, 44458.
(14) Al Zoubi, W.; Min, J. H.; Ko, Y. G. Hybrid organic-inorganic coatings via electron transfer behaviour. *Sci. Rep.* **2017**, *7*, 7063.
(15) Bai, A.; chen, Z.-J. Effect of Electrolyte Additives on Anti-corrosion Ability of Micro-Arc Oxide Coatings Formed on Magnesium Alloy AZ91D. *Surf. Coat. Technol.* **2009**, *203*, 1956−1963.
(16) Goto, T.; Iwaki, T.; Ito, Y. Electrochemical Formation of AlN in Molten LiCl-KCl-Li_3N Systems. *Electrochim. Acta* **2005**, *50*, 1283−1288.
(17) Wang, K.; Byeon, S. S.; Jung, Y. G.; Koo, B. H. Effect of the Nitrogen Inducing Agents on the Corrosion Behavior of the Oxide Coatings Prepared by Electrolytic Plasma Processing on the Al2021 Alloy. *Ceram. Int.* **2012**, *38*, S669−S672.
(18) Wang, Y.; Wang, M.; Jiang, Z. Synthesis and Characterization of Aluminum Nitride Ceramic Coating on Aluminum Alloy by Plasma Electrolytic Oxidation in $CO(NH_2)_2$ Electrolyte. *Adv. Mater. Res.* **2012**, *557*−*559*, 1664−1667.
(19) Yeh, S. C.; Tsai, D. S.; Guan, S. Y.; Chou, C. C. Influences of Urea and Sodium Nitrite on Surface Coating of Plasma Electrolytic Oxidation. *Appl. Surf. Sci.* **2015**, *356*, 135−141.
(20) Albella, J. M.; Montero, I. J.; Martinez-Duart, J. M. A Theory of Avalanche Breakdown During Anodic Oxidation. *Electrochim. Acta* **1987**, *32*, 255−258.
(21) Li, Z.; Yuan, Y.; Jing, X. Effect of Current Density on the Structure, Composition and Corrosion Resistance of Plasma Electrolytic Oxidation Coatings on Mg-Li Alloy. *J. Alloys Compd.* **2012**, *541*, 380−391.
(22) Arrabal, R.; Matykina, E.; Hashimoto, T.; Skeldon, P.; Thompson, G. E. Characterization of AC PEO Coatings on Magnesium Alloys. *Surf. Coat. Technol.* **2009**, *203*, 2207−2220.
(23) White, L.; Koo, Y.; Neralla, S.; Sankar, J.; Yun, Y. Enhanced Mechanical Properties and Increased Corrosion Resistance of a Biodegradable Magnesium Alloy by Plasma Electrolytic Oxidation PEO. *Mater. Sci. Eng., B* **2016**, *208*, 39−46.
(24) Yao, Z.; Ju, P.; Xia, Q.; Wang, J.; Su, P.; Wei, H.; Li, D.; Jiang, Z. Preparation of Thermal Control Coatings on Mg-Li Alloys by Plasma Electrolytic Oxidation. *Surf. Coat. Technol.* **2016**, *307*, 1236−1240.
(25) Guo, F.; Ye, K.; Du, M.; Huang, X.; Cheng, K.; Wang, G.; Cao, D. Electrochemical Impedance Analysis of Urea Electro-Oxidation Mechanism on Nickel Catalyst in Alkaline Medium. *Electrochim. Acta* **2016**, *210*, 474−482.
(26) Khaselev, O.; Weiss, D.; Yahalom, J. Structure and Composition of Anodic Films Formed On Binary Mg-Al Alloys In KOH-Aluminate Solution Under Continuous Sparking. *Corros. Sci.* **2001**, *43*, 1295−1307.
(27) Li, X.; Liu, X. Y.; Luan, B. L. Corrosion and Wear Properties of PEO Coating of PEO Coating Formed on AM60B Alloy in $NaAlO_2$ Electrolytes. *Appl. Surf. Sci.* **2011**, *257*, 9135−9141.
(28) Wang, X.; Yang, H.; Wang, F. A Cationic Gemini-Surfactant as Effective Inhibitor for Mild Steel in HCl Solutions. *Corros. Sci.* **2010**, *52*, 1268−1276.
(29) Li, W.; Li, D. Y. Influence of Surface Morphology on Corrosion and Electronic Behavior. *Acta Mater.* **2006**, *54*, 445.
(30) Hong, T.; Nagumo, M. Effect of Surface Roughness on Early Stages on Pitting Corrosion of 301 Stainless Steel. *Corros. Sci.* **1997**, *39*, 1665.
(31) Koebel, M.; Elsener, M.; Kleemann, M. Urea-SCR: A Promising Technique to Reduce NOx Emissions from Automotive Diesel Engines. *Catal. Today* **2000**, *59*, 335−345.
(32) Liang, J.; Guo, B. G.; Tian, J.; Liu, H. W.; Zhou, J. F.; Liu, W. M.; Xu, T. Effects of $NaAlO_2$ on Structure and Corrosion Resistance of Microarc Oxidation Coatings Formed on AM60B Magnesium Alloy in Phosphate-KOH Electrolyte. *Surf. Coat. Technol.* **2005**, *199*, 121−126.
(33) Ko, Y. G.; Lee, B. U.; Shin, D. H.; et al. An Electrochemical Analysis of AZ91 Mg Alloy processed by Plasma Electrolytic Oxidation Followed by Static Annealing. *J. Alloys Compd.* **2011**, *509*, S468−S472.
(34) Morlidge, J. R.; Skeldon, P.; Thompson, G. E.; Habazaki, H.; Shimizu, K.; Wood, G. C. Gel Formation and the Efficiency of Anodic Film Growth on Aluminium. *Electrochim. Acta* **1999**, *44*, 2423−2435.
(35) Zhang, Y.; Yan, C.; Wang, F.; Li, W. Electrochemical Behaviour of Anodized Mg alloy AZ91D in Chloride Containing Aqueous Solution. *Corros. Sci.* **2005**, *47*, 2816−2831.
(36) Jamesh, M.; Kumar, S.; Sankara Narayanan, T. S. N. Corrosion Behavior of Commercially Pure Mg and ZM21 Mg alloy in Ringer's solution-Long Term Evaluation by EIS. *Corros. Sci.* **2011**, *53*, 645−654.
(37) Gao, Y.; Yerokhin, A.; Matthews, A. Deposition and Evaluation of Duplex Hydroxyapatite and Plasma Electrolytic Oxidation Coatings on Magnesium. *Surf. Coat. Technol.* **2015**, *269*, 170−182.
(38) Baril, G.; Pebere, N. The Corrosion of Pure Magnesium in Aerated and Deaerated Sodium Sulphate Solutions. *Corros. Sci.* **2001**, *43*, 471−484.

DOI: 10.1021/acsami.7b05773
ACS Appl. Mater. Interfaces 2017, 9, 28967−28979

(39) Baril, G.; Galicia, G.; Deslouis, C.; Pebere, N.; Tribollet, B.; Vivier, V. An Impedance Investigation of The Mechanism of Pure Magnesium Corrosion in Sodium Sulphate Solution. *J. Electrochem. Soc.* **2007**, *154*, C108−C113.
(40) Liang, J.; Srinivasan, P. B.; Blawert, C.; Störmer, M.; Dietzel, W. Electrochemical Corrosion Behaviour of Plasma Electrolytic Oxidation Coatings on AM50 Magnesium Alloy Formed in Silicate and Phosphate Based Electrolytes. *Electrochim. Acta* **2009**, *54* (14), 3842−3850.
(41) Song, Y.; Shan, D.; Chen, R.; Han, E. H. Corrosion Characterization of Mg-8Li Alloy in NaCl Solution. *Corros. Sci.* **2009**, *51* (5), 1087−1094.
(42) Boggs, B. K.; King, R. L.; Botte, G. G. Urea electrolysis: Direct Hydrogen Production from Urine. *Chem. Commun.* **2009**, *32*, 4859−4861.
(43) King, R. L.; Botte, G. G. Investigation of Multi-Metal Catalysts for Stable Hydrogen Production via Urea Electrolysis. *J. Power Sources* **2011**, *196*, 9579−9584.
(44) Zhang, F.; Zhang, C.; Song, L.; Zeng, R.; Li, S.; Cui, H. Fabrication of the Superhydrophobic Surface on Magnesium Alloy and Its Corrosion Resistance. *J. Mater. Sci. Technol.* **2015**, *31*, 1139−1143.
(45) Zheng, T.; Hu, Y.; Zhang, Y.; Pan, F. Formation of a Hydrophobic and Corrosion Resistant Coating on Magnesium Alloy via a one-step Hydrothermal method. *J. Colloid Interface Sci.* **2017**, *505*, 87−95.
(46) Wu, G. S.; Dai, W.; Zheng, H.; Wang, A. Y. Improving Wear Resistance and Corrosion Resistance of AZ31 Magnesium Alloy by DLC/AlN/Al Coating. *Surf. Coat. Technol.* **2010**, *205*, 2067−2073.
(47) Zhang, L.; Mohammed, E. A. A.; Adriaens, A. Synthesis and Electrochemical Behavior of a Magnesium Fluoride-Polydopamine-Stearic Acid Composite Coating on AZ31 Magnesium Alloy. *Surf. Coat. Technol.* **2016**, *307*, 56−64.
(48) Hernández-Barrios, C. A.; Cuao, C. A.; Jaimes, M. A.; Coy, A. E.; Viejo, F. Effect of the Catalyst Concentration, the Immersion Time and the Aging Time on the Morphology, Composition and Corrosion Performance of TEOS-GPTMS Sol-Gel Coatings Deposited on the AZ31 Magnesium Alloy. *Surf. Coat. Technol.* **2017**, *325*, 257−269.
(49) Wu, G. S.; Zeng, X. Q.; Yuan, G. Y. Growth and Corrosion of Aluminum PVD Coating on AZ31 Magnesium Alloy. *Mater. Lett.* **2008**, *62*, 4325−4327.
(50) Pompa, L.; Rahman, Z. U.; Munoz, E.; Haider, W. Surface Characterization and Cytotoxicity Response of Biodegradable Magnesium Alloys. *Mater. Sci. Eng., C* **2015**, *49*, 761−768.
(51) Zhao, J.; Xie, X.; Zhang, C. Effect of the Graphene Oxide Additive on the Corrosion Resistance of the Plasma Electrolytic Oxidation Coating of the AZ31 Magnesium Alloy. *Corros. Sci.* **2017**, *114*, 146−155.
(52) Lim, T. S.; Ryu, H. S.; Hong, S. H. Electrochemical Corrosion Properties of CeO_2-Containing Coatings on AZ31 Magnesium Alloys Prepared By Plasma Electrolytic Oxidation. *Corros. Sci.* **2012**, *62*, 104−111.
(53) Huang, Q. A.; Hui, R.; Wang, B.; Zhang, J. A Review of AC Impedance Modeling and Validation in SOFC Diagnosis. *Electrochim. Acta* **2007**, *52*, 8144−8164.
(54) Durdu, S.; Aytac, A.; Usta, M. Characterization and Corrosion Behavior of Ceramic Coating on Magnesium by Micro-Arc Oxidation. *J. Alloys Compd.* **2011**, *509*, 8601−8606.
(55) Durdu, S.; Usta, M. Characterization and Mechanical Properties of Coatings on Magnesium by Micro Arc Oxidation. *Appl. Surf. Sci.* **2012**, *261*, 774−782.
(56) Guo, H. F.; An, M. Z.; Huo, H. B.; Xu, S.; Wu, L. J. Microstructure Characteristic of Ceramic Coatings Fabricated on Magnesium Alloys by Micro-Arc Oxidation In Alkaline Silicate Solutions. *Appl. Surf. Sci.* **2006**, *252* (22), 7911−7916.
(57) Yan, W.; Wang, D.; Botte, G. G. Electrochemical Decomposition of Urea with Ni-Based Catalysts. *Appl. Catal., B* **2012**, *127*, 221−226.
(58) Yan, W.; Wang, D.; Botte, G. G. Nickel and Cobalt Bimetallic Hydroxide Catalysts for Urea Electro-Oxidation. *Electrochim. Acta* **2012**, *61*, 25−30.
(59) Caton, J. A.; Siebers, D. L. Comparison of Nitric Oxide Removal by Cyanuric Acid and by Ammonia. *Combust. Sci. Technol.* **1989**, *65*, 277−293.
(60) Rota, R.; Antos, D.; Zanoelo, E. F.; Morbidelli, M. Experimental and Modeling Analysis of the NOxOUT process. *Chem. Eng. Sci.* **2002**, *57*, 27−38.
(61) Schaber, P. M.; Colson, J.; Higgins, S.; Thielen, D.; Anspach, B.; Brauer, J. Thermal Decomposition (Pyrolysis) of Urea in an Open Reaction Vessel. *Thermochim. Acta* **2004**, *424*, 131−142.
(62) Serov, A.; Kwak, C. Direct hydrazine Fuel Cells: A review. *Appl. Catal., B* **2010**, *98*, 1−9.
(63) Abernethy, G. A. Generation of Semicarbazide from Natural Azine Development in Foods, Followed by Reaction with Urea Compounds. Food Addit. Contam Part A Chem. Anal. Control Expo. *Food Addit. Contam., Part A* **2015**, *32*, 1416−1430.
(64) Chen, H.; Chen, D. Z.; Fan, S.; Hong, L.; Wang, D. SNCR De-NOx Within a Moderate Temperature Range Using Urea-Spiked Hydrazine Hydrate as Reductant. *Chemosphere* **2016**, *161*, 208−218.

DOI: 10.1021/acsami.7b05773
ACS Appl. Mater. Interfaces 2017, 9, 28967−28979